Journal of the Korean Nuclear Society
Volume 34, Number 3, pp.218~231, June, 2002

A Control Volume Scheme for Three-Dimensional Transport: Buffer and Matrix Effects on a Decay Chain Transport in the Repository

Y.M. Lee, Y.S. Hwang, S.G. Kim, and C.H. Kang
Korea Atomic Energy Research Institute
150 Dukjin-dong, Yuseung-gu, Daejon 305-353, Korea
ymlee@kaeri.re.kr

(Received October 22, 2001)

Abstract

Using a three-dimensional numerical code, B3R developed for nuclide transport of an arbitrary length of decay chain in the buffer between the canister and adjacent rock in a high-level radioactive waste repository by adopting a finite difference method utilizing the control-volume scheme, some illustrative calculations have been done. A linear sorption isotherm, nuclide transport due to diffusion in the buffer and the rock matrix, and advection and dispersion along thin rigid parallel fractures existing in a saturated porous rock matrix as well as diffusion through the fracture wall into the matrix is assumed. In such kind of repository, buffer and rock matrix are known to be important physico-chemical barriers in nuclide retardation. To show effects of buffer and rock matrix on nuclide transport in HLW repository and also to demonstrate usefulness of B3R, several cases of breakthrough curves as well as three-dimensional plots of concentration isopleths associated with these two barriers are introduced for a typical case of decay chain of $^{234}U \rightarrow ^{230}Th \rightarrow ^{226}Ra$, which is the most important chain as far as the human environment is concerned.

Key Words : nuclide transport, safety assessment, HLW repository, 3-D numerical model

Notation

$2b$ = fracture aperture, [L]

b = super- and subscripts denoting the buffer

b,p = super- and subscripts denoting the buffer and the matrix together

$\tilde{c}_l(t)$ = concentration of nuclide l at the inlet, [ML^{-3}]

c_E, c_W, c_N, c_S, c_F, c_B c_P = concentrations at each grid point as shown in Figs. 4 and 5, [ML^{-3}]

c_l = concentration of nuclide l, [ML^{-3}]

c_{l_0} = initial concentration of nuclide l at the inlet, [ML^{-3}]

D^* = molecular diffusion coefficient in water, [L^2T^{-1}]

$D_{b\rightarrow f}$, $D_{f\rightarrow b}$ = interface diffusion coefficients through the buffer-fracture and the fracture-buffer interfaces as defined in Appendix II, [L^2T^{-1}]

$D_{b\rightarrow p}$, $D_{p\rightarrow b}$ = interface diffusion coefficients

through the buffer-matrix and the matrix-buffer interfaces as defined in Appendix II, [L^2T^{-1}]

$D_{f\to p}$, $D_{p\to f}$ = interface diffusion coefficients through the fracture-matrix and the matrix-fracture as defined in Appendix II, [L^2T^{-1}]

D_L = longitudinal hydrodynamic dispersion coefficient in the fracture, further expressed as, $D_L = \alpha_L \cdot v + D^*$, [$L^2T^{-1}$]

D_{ty}, D_{tz} = transverse hydrodynamic dispersion coefficients in the fracture in the y- and z-direction, respectively, [L^2T^{-1}]

e, w, n, s, f, b = control volume faces as defined in Figs. 4 and 5

E, W, N, S, F, B, P = subscripts for grid point concentration as shown in Figs. 4 and 5

f = super- and subscripts denoting the fracture

J = total flux in the fracture as defined in Appendix I, [$ML^{-2}T^{-1}$]

l = subscript denoting parent nuclide

l-1 = subscript denoting daughter nuclide

p = super- and subscripts denoting the matrix

R_l = retardation coefficient in the fracture for nuclide *l*

R_{l_b}= retardation coefficient in the buffer for nuclide l

R_{l_p}= retardation coefficient in the matrix for nuclide *l*

t = elapsed time, [T]

$t_{0.5}$ = half-life of nuclide, [T]

v = groundwater velocity in the fracture, [LT^{-1}]

x, y, z = coordinates as defined in Fig. 1, [L]

x_c = radius of canister (see Fig. 2), [L]

x_b = outer radius of buffer region (x_b - x_c = buffer thickness), [L]

x_L, y_L = distances to the outlet boundary in the x- and y-direction, respectively, [L]

α_L = dispersivity along the fracture, [L]

$(\delta x)_e$, $(\delta x)_w$, $(\delta y)_s$, $(\delta y)_n$, $(\delta z)_f$, $(\delta z)_b$ = distances between nodes as defined in Fig. 5(b), [L]

$(\delta x)_{e+}$ = distance as defined in Fig. 5(b), [L]

Δ_{xi}, Δ_{yj}, Δ_{zk} = spatial discretization increment in the x-, y-, and z-direction, respectively [L]

Δ_t = temporal increment, [T]

λ_l = decay constant of nuclide l, [T^{-1}]

θ_b = porosity of the buffer

θ_f = porosity of the fracture set to 1.0

θ_p = porosity of the matrix

$(\theta_b D_x^b)$, $(\theta_b D_y^b)$, $(\theta_b D_z^b)$ = effective diffusion coefficients in the buffer in the x- and y-, and z-direction, respectively, [L^2T^{-1}]

$(\theta_p D_x^p)$, $(\theta_b D_y^p)$, $(\theta_p D_z^p)$ = effective diffusion coefficients in the matrix in the x- and y-, and z-direction, respectively, [L^2T^{-1}]

1. Introduction

The potential repository for the final disposal of high-level radioactive waste (HLW) is very likely to be located in deep geological formation in Korea. This kind of concept would be similar to that for Swedish KBS-3 (1983) in which the disposal of spent fuel assemblies in canisters individually emplaced in vertical deposition holes is considered. In this case the buffer material is designed to have low permeability to delay the contact of the waste by groundwater as well as to retard nuclides transporting to the host rocks. Also the significance of rock matrix in the host rock has also been noted in the literature (e.g., Neretnieks, 1980) showing a few hundred meters of good rock could be a most effective barrier for most important nuclides in HLW.

Also for such HLW repository located in deep geological formations, behavior of chain decaying nuclide in geological media has been an important topic in assessing its performance.

However, unfortunately, only a limited number of analytical works for limited modeling system are available relating the multi-member chain decay transport. In order to overcome limitations associated with analytical models, many numerical approaches have been developed for decades

(e.g., Grisak and Pickens, 1980; Huyakorn et al., 1983a; Lee et al., 1989; Kennedy and Lennox, 1995). However, many of these do not provide an exact solution or are not capable of adequately modeling transport for decay chains of an arbitrary length, which is essential in analysis of radioactive waste disposal systems. As for the decay chain models, although Sudicky and Frind (1984) developed an exact analytical solution for two-member decay chain transport in a fractured medium, neglecting hydrodynamic dispersion along the fracture, a complete analytical solution in a closed form may not yet available for multi-member chain decay and transport, whereas many solutions for a porous medium without matrix diffusion or for the media having rather simple geometry have been found in the literature (e.g., Harada et al., 1980; Lung, 1986; Gureghian, 1987; Kang, 1989).

Since Huyakorn et al. (1983b) dealt with decay chain transport in a fractured porous medium by utilizing a finite element technique, various different kinds of numerical scheme have been introduced (e.g. Yamashita and Kimura, 1990 ; Lee and Lee, 1995).

Recently a series of studies associated with chain decay transport have been done numerically by authors (Lee et al., 1993; Lee et al., 1995; Lee and Lee, 1995; Lee et al, 1996; Lee and Kang, 1997; Lee et al, 1997).

Also, a two-dimensional finite-difference numerical solution for nuclide transport of an 'arbitrary decay chain length' (i.e., multi-member chain decay) through a buffer and adjacent fractured porous medium by utilizing a control volume method has been developed and the exactness of this solution by comparisons with available analytical solutions has been investigated in a series of works by Lee and Kang (1999a; 1999b) and Lee et al. (1999).

The purpose of this paper is to extend the previous work by considering the media as a three-dimensional modeling domain and visualize how nuclides can be transported across the buffer-matrix and buffer-fracture interfaces around a canister. In other words, the primary application of the model and the code is to evaluate and to visualize the effect of nuclide behavior in the HLW repository, the model in this paper accounts for chain decay transport in buffer and fractured porous media. Adopting this model a computer code named B3R has been developed.

The examples presented in this paper are limited to and concerned with transport of nuclide having decay chains and its effect in the presence of buffer and rock matrix diffusion, considering in-growth due to daughter nucides' decay even though any in-depth sensitivity studies in relation to buffer thickness and matrix properties are not dealt with to show the importance of such barriers in view of HLW repository safety.

2. Three-Dimensional Numerical Model

Soon after nuclides escaped from a penetrated canister having HLW in it, they will diffuse through the buffer material around the canister and eventually will be transferred to the host rock. Fractures in the host rock around the buffer may intersect disposal holes for canister providing groundwater pathways for the hydrogeologic nuclide transport due to advection, whereas porous rock matrix interfaced with buffer will provide diffusive transport pathways for nuclides (se Fig. 1). Since fractures having permeabilities several orders of magnitude higher than the rock matrix itself provide a main hydrogeologic pathway for the transport of the nuclide into the far-field region, the assumption that the rock matrix surrounding the buffer is impervious to nuclide transport has commonly been made. However, recently, studies show that the nuclides

are available to diffuse freely across the buffer-matrix boundary and the matrix can ply an important role to retard the nuclides requiring rather in depth studies involved. However, such an approach is difficult to be handled with an analytical method due to the complexity of domain.

The physical system of the fractured rock modeled here is similar to that treated in many works (e.g., Sudicky and Frind, 1982; Sudicky and Frind, 1984; Lee et al., 1989; Lee et al., 1993; Lee and Lee, 1995; Lee and Kang, 1997). In these models thin rigid parallel fractures are embedded in a saturated porous rock matrix by approximating the fractured porous medium as three-dimensional parallel fracture-embedded rock block. The buffer is modeled as a common three-dimensional porous medium as shown in Fig. 1. The geometry and dimension of the modeled domain are also shown in Fig. 2.

Assuming a linear sorption isotherm, transport for the nuclide l in a saturated fracture can be described by

$$R_l\frac{\partial c_l}{\partial t}+\lambda_l c_l R_l=\frac{\partial}{\partial x}\left(D_L\frac{\partial c_l}{\partial x}-vc_l\right)+\frac{\partial}{\partial y}\left(D_{tr}\frac{\partial c_l}{\partial y}\right)+\frac{\partial}{\partial z}\left(D_{tz}\frac{\partial c_l}{\partial z}\right)+\lambda_{l-1}c_{l-1}R_{l-1},$$
$$x_b\cos\phi\le x\le x_L\left(0\le\phi\le\tfrac{\pi}{2}\right),\ 0\le y\le b,\begin{cases}x_b\sin\phi\le z\le x_b\cap 0\le x<x_b\\ 0\le z\le x_b\cap x\ge x_b\end{cases},\ t>0. \quad (1)$$

Also, unlike fracture, assuming that no advective transport takes place in the buffer as well as in the matrix, the governing equation for nuclide transport in such porous media is

$$R_l^{b,p}\frac{\partial c_l}{\partial t}+\lambda_l c_l R_l^{b,p}=\frac{\partial}{\partial x}\left(\theta_{b,p}D_x^{b,p}\frac{\partial c_l}{\partial x}\right)+\frac{\partial}{\partial y}\left(\theta_{b,p}D_y^{b,p}\frac{\partial c_l}{\partial y}\right)+\frac{\partial}{\partial z}\left(\theta_{b,p}D_z^{b,p}\frac{\partial c_l}{\partial z}\right)+\lambda_{l-1}c_{l-1}R_{l-1}^{b,p},$$
$$\begin{cases}x_r\cos\phi<x<x_c\cos\phi+(x_b-x_r),\ 0<y<y_L,\ x_r\sin\phi<z<x_b\cos\omega,\ t>0; & \text{for bufffer}\\ x_b\cos\phi<x<x_L,\ b<y<y_L,\ x_b\sin\phi<z<x_b,\ t>0; & \text{for matrix.}\end{cases} \quad (2)$$

The discretized domain for the buffer and fractured porous media is as depicted in Fig. 3, where the boundary conditions are zero concentration gradient (Neuman-type) boundary conditions as represented in Eq. (3) at all boundaries only except at the canister surface interface, *i.e.*, except for the inlet:

$$\frac{\partial c_l}{\partial x}=0,\quad x=x_L \quad (3)$$

For initial and boundary conditions associated with the inlet of the buffer, nuclide decay and transformation of the parent nuclide into its daughter products are considered together by Bateman's decaying source. Therefore the concentration at the inlet boundary for the l-th component of the decay chain, $\tilde{c}l(t)$, which is written as

$$\tilde{c}_l(t)=\sum_{m=1}^{l}B_{lm}e^{-\lambda_m t} \quad (4)$$

where

$$B_{lm}=\sum_{n=1}^{m}c_n^0\prod_{k=n}^{l-1}\lambda_k\left\{\prod_{\substack{j=n\\ j\ne m}}^{l}(\lambda_j-\lambda_m)\right\}^{-1} \quad (5)$$

and c_l^0 denotes the initial concentration due to inventory at the inlet.

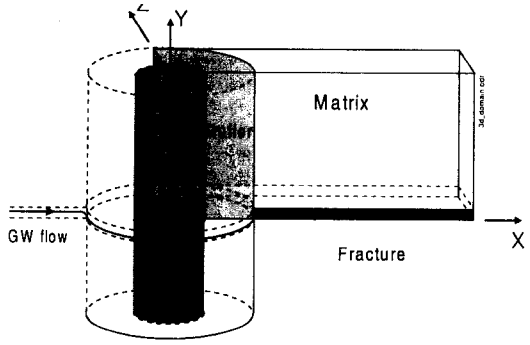

Fig. 1. Schematic View of a Deposition Hole Intersected by a Fracture in a Potential HLW Repository Tunnel

To derive a three-dimensional discretization equation by control volume approach, first of all, a grid-point cluster is introduced. (See Figs. 3 and 4.) The modeled domain is divided into variably sized control volumes, each of which has a central grid point, *P* located in the geometrical center of the control volume. The control volume faces are

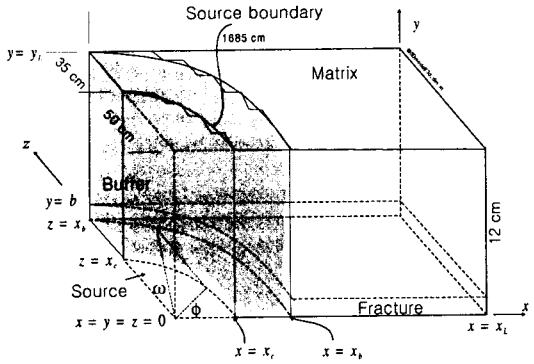

Fig. 2. The Dimension of the Modeled Domain

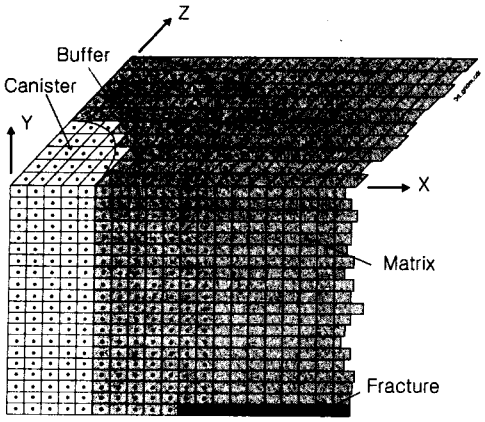

Fig. 3. Three-dimensional Discretization of the Domain

not necessarily located equidistant from the each adjacent node. Once the control volumes have been defined, the concentration value is evaluated at each node. The full description for the discretization procedure is represented in detail in Appendix I.

In order to avoid a discontinuity in physical properties within a control volume, discontinuities in the medium, such as at the no flux boundary and the fracture-matrix boundary, are recommended to be located at control volume faces. Although it leads to the half-sized control volumes around the grid points, by postulating a grid point at the face

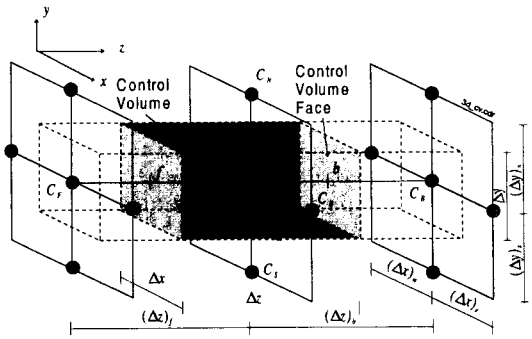

Fig. 4. A Control Volume with Notations

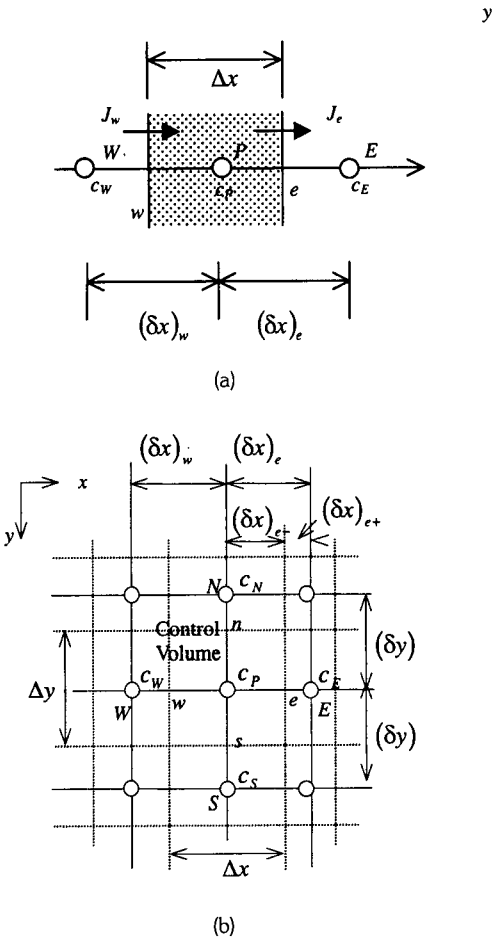

Fig. 5. (a) Steady State One-dimensional Consideration for the Flux in the Fracture (in the x-direction); (b) Two-dimensional View of Control Volume in the x-y Plane

Table 1. Spatial Increments for the Control Volume

Δx_i, cm i=1, 2, 3,..., 100	7(i=1...5), 10(i=6...10), 15(i=11...50), 20(i=51...100)
Δy_j, cm j=1, 2, 3,..., 20	0.006($=b/2$), 0.009, 0.015, 0.025, 0.045, 0.07, 0.13, 0.25, 0.45, 1(j=10...20)
Δz_k, cm j=1, 2, 3,..., 10	7(k=1...5), 10(k=6...10)

Table 2. Nuclide Data

Nuclide	$t_{0.5}$, yr	R_l, R^b_l, R^p_l	c_l^0
^{234}U	2.47×10^5	120.	$c_0 = 1.0$
^{230}Th	$8. \times 10^4$	1500.	$c_0 = 0.0$
^{226}Ra	1600.	300.	$c_0 = 0.0$

having control volume of zero thickness, the need for special discretization at discontinuities can be eliminated.

The solutions of the algebraic equations (A7) and (A8) are then obtained using a simple Gauss-Seidel iteration scheme.

2.2. Retardation Effects of the Buffer and the Rock Matrix on Transport

Any works associated with demonstration of the validity and relative accuracy of the scheme developed associated with this study has not shown. Since several examples which is limited to two-dimensional work for the fractured rock medium have been considered in comparisons with available analytical solutions through other works (e.g., Lee and Kang, 1999a), no further verification for current three-dimensional model, which is an extended version of two-dimensional model, are not made through this study.

As seen in the Table 1, the number of control volumes used is 100 along the fracture axis in the x-direction, 20 in the y-direction into the matrix, and 10 in the horizontal z-direction, giving a total of $100 \times 20 \times 10$ control volumes.

Parameters used are also listed in Tables 2 and 3.

In Figs. 6 and 7, both of which take zero buffer thickness, the effects on concentrations of $^{234}U \rightarrow ^{230}Th \rightarrow ^{226}Ra$ chain, normalized to parent nuclide concentration in the fracture at the distance of x = 6.775m in view of matrix diffusion in the host rock are shown. Fig. 6 which does not consider any retardation effect throughout all media show a little higher values of concentration from early time, compared to the case retardation effects are considered, as represented in Fig. 7. Nuclide concentrations of daughters for the case of no retardations throughout the media have the quite higher values earlier than those retarded as well. The parameters of the calculation are listed on the figure, and all these parameter are fixed through calculations in this study at values given. In the figures, solid lines and dotted lines represent the concentrations of parent nuclide and its daughters, respectively normalized to the parent concentration as a function of time.

As shown in both figures the concentration of parent nuclide, ^{234}U is almost constant after reach at the peak until the decay effect becomes

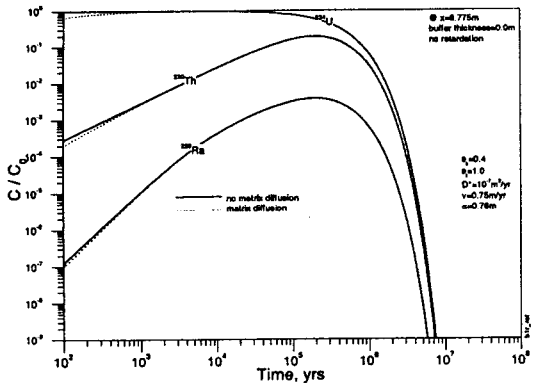

Fig. 6. Breakthroughs as a Function of Time at x = 6.775m in the Fracture, Showing Comparison of the Cases of Matrix Diffusion Available or Not (no retardation)

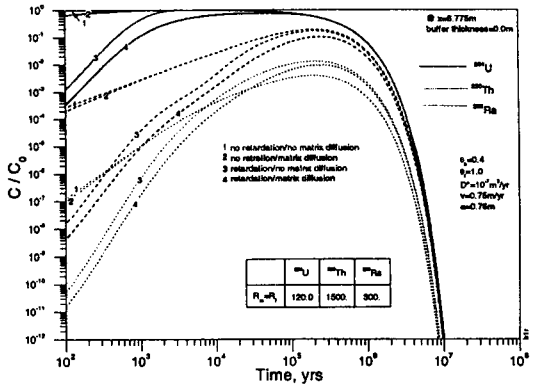

Fig. 8. Breakthroughs as a Function of Time at x = 6.775m in the Fracture in Case of No Buffer

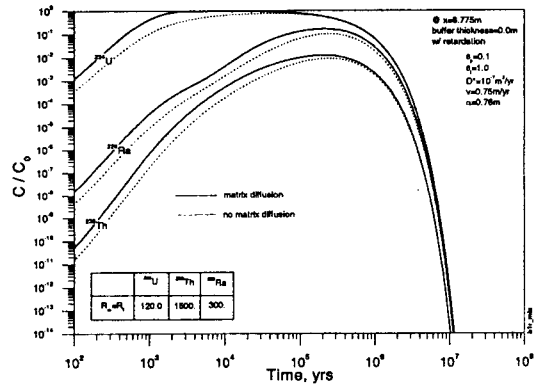

Fig. 7. Breakthroughs as a Function of Time at x = 6.775m in the Fracture, Showing Comparison of the Cases of Matrix Diffusion Available or Not (retardation)

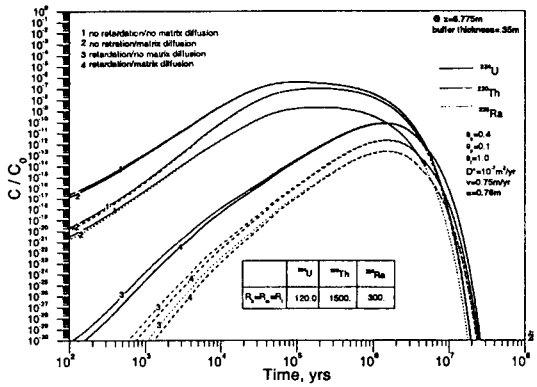

Fig. 9. Breakthroughs as a Function of Time at x = 6.775m in the Fracture, Showing Comparison of the Cases of Matrix Diffusion and Retardation Available or Not

pronounced. The concentration of daughters, ^{230}Th and ^{226}Ra increase from zero to the highest peak values about at several 10^5 years, and then decrease as the concentration of ^{234}U decreases.

More specifically, Fig. 6, with the presence of matrix diffusion as parameter, shows how extreme cases of existence and non-existence of matrix diffusion can result for the transport of nuclides. It turns out that even when there is matrix diffusion available during transport along the fracture, if there is no retardation, no remarkable change of the concentration breakthrough are not found. This kind of phenomenon also seems to be true for the other case that retardation is considered, as seen in Fig. 7 that shows the same thing as in Fig. 6 only with presence of retardation.

All shapes of breakthrough curves do not greatly matter matrix diffusion effect for both cases.

However, in contrast, for all cases retardation is considered, curves considering matrix diffusion show about a half order of magnitude of lower concentrations than those considering no matrix diffusion.

In Fig. 8, which combines Fig. 6 and Fig. 7 together for the comparison purpose, retardation effects are so remarkable that it shows for the case of retardation throughout the media the peak concentration of the retarded nuclides are delayed very much and even duration of the peak narrows down.

One can also see that, in the case of presence of retardation, parent nuclide, ^{234}U shows its peak earlier than the other two daughter nuclides due to its relatively smaller retardation coefficient.

Through the study several effects on consideration of matrix diffusion in the host rock and retardation in all media are investigated. Among them, in Fig. 9, which takes 35cm of buffer thickness, several normalized concentrations in the fracture at the distance of x = 6.775m are shown.

First of all, the importance of retardation can be revealed when comparing all results with those in which retardation is assumed absent. In absence of matrix diffusion the breakthrough are not greatly changed from the results with matrix diffusion, which is the similar behavior as seen in Fig. 6 for the case of no buffer.

Fig. 10 shows the breakthrough curves comparing the results in the presence of buffer with those in the absence of buffer. Both cases are assumed that both matrix diffusion and the retardation throughout all media take place together. It is easily seen that such phenomena decrease about four orders of magnitude of peak values of parent nuclide concentration as well as daughters'. This means, as a summary, to make such reduction more effective, one can only expect to increase the buffer thickness with large

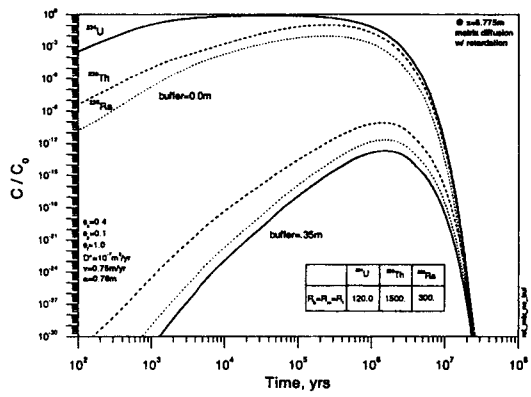

Fig. 10. Breakthroughs as a Function of Time at x = 6.775m in the Fracture, Showing Comparison Between Each Case of Buffer Considered or Not

retardation coefficient in the buffer, although any in-depth sensitivity studies are not made for the study for the time being. However, matrix diffusion are not greatly and relatively expected to reduce the peak concentration for any case of retardation is available or not, even though the case with the same retardation coefficient values for the same nuclides are taken for the buffer, the rock matrix, and the fracture in case retardation should be considered. What else to be discussed is about these figures for the case of consideration of buffer is very similar to plots for the case of no buffer.

2.3. Some 3-Dimensional Plots Showing Nuclide Behavior in the Barriers

The volume or face plots of concentrations of parent nuclide (^{234}U) in the media around the quartile section of a canister, normalized to its initial concentration at the inlet boundary surface of the canister where $\tilde{c}_i$ is to be decayed time-dependently according to Bateman equation (Eqs. (4) and (6) in Table 4), as a function of distances in

Table 3. Parameters Used

Parameter	Value
$2b$	120μm
θ_b	0.1
θ_f	1.0
θ_p	0.4
θ_L	0.76 m
v	0.75 m/yr
$(\theta D_x^p) = (\theta D_y^p) = D^*$	8.64×10^{-6} m^2/yr
D_L	$\alpha_L \cdot v + D^*$
x_c	50cm
x_b	85cm
buffer thickness (= x_b - x_c)	35cm
^xL	16.85m
^yL	12cm
^zL	85cm

the x-, y- and z-directions at time equal to 8×10^3 years are shown in Figs. 11 and 12. Instead of plots for the whole family of decay chain of $^{234}U \rightarrow ^{230}Th \rightarrow ^{226}Ra$, only parent cases are introduced since it is emphasized that the solution and associated computer code, B3R developed through this study are not limited by the specific number of members in the chain and that decay chain was not dealt with for the time being especially for the illustrative purpose avoiding complexity in plots.

Fig. 11 shows the isopleths in case there are matrix diffusions both from the buffer and the fracture without any retardation through whole media are considered. On the other hand, Fig. 12 shows each case when retardation and matrix diffusion are involved.

Plots for ^{234}U for the case retardations are considered for all media (Fig. 12a) show rather slow concentration isopleths, compared to the baseline case (Fig. 11). For the case there is no transverse matrix diffusion through the fracture wall, Fig. 12b shows their dominant concentration isopleths along the fracture (around y = 0).

By investigating further more for Fig, 11 and Figs, 12(a) and 12(b), one can easily see the retardation effect from Fig. 12(a), compared to Fig. 11. Also, very naturally, it is shown that ^{234}U in Fig. 11 travels relatively faster than ^{234}U in Fig. 12(b). This is because the nuclides entering the fracture are taken away by advection and dispersion due to groundwater flow takes place only in the fracture although there is no loss term due to matrix diffusion into the matrix from the fracture unlike the case depicted in Fig. 11. For all cases nuclides are supplied from the buffer into the rock as well as through the inlet of the fracture.

In summary, with the advection-dispersion parameters chosen, these calculations visualizes the isopleths that ^{234}U travels physically well around the canister, buffer and other surrounding media.

2.4. Concluding Remarks

For more effective calculation, varying temporal steps according to the calculation time can be used through out the computation. After some numerical experiments through a series of the

Table 4. Initial and Boundary Conditions

I.C.	$c_l(x, y, z; t = 0), \quad l = 1, 2, 3$	(5)
B.C. (@ inlet)	$c_l(x=x_c \cos\phi, 0 \le y \le y_L, 0 \le z \le x_b; t) = \tilde{c}_l, \quad l = 1, 2, 3, \ldots$	(6a)
	$vc_l(x=x_c \cos\phi, 0 \le y \le y_L, 0 \le z \le x_b; t) - D_L = \frac{\partial c_l}{\partial y} = v\tilde{c}_l \quad l = 1, 2, 3, \ldots$	(6b)

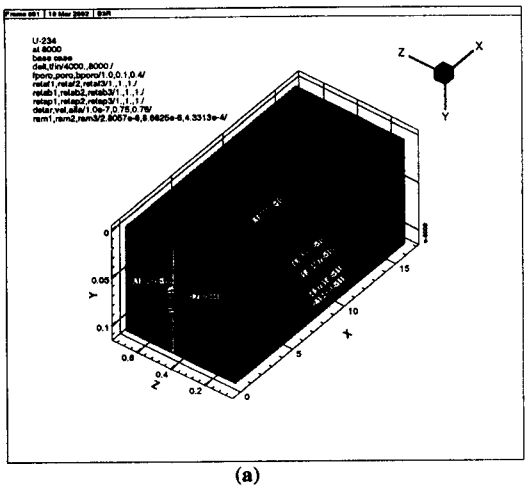

(a)

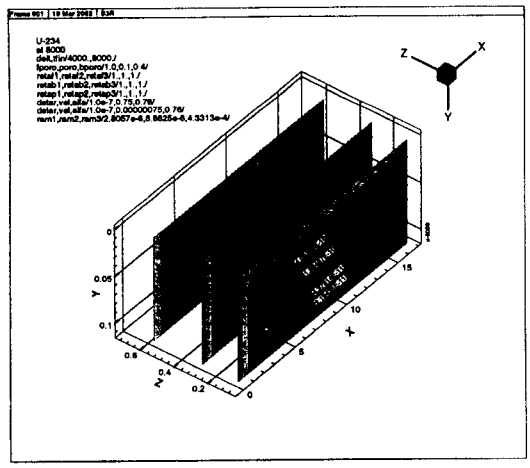

(b)

Fig. 11. Volume Plot (a) and Face Plot (b) for ^{234}U at Time of 8×10^3 Years

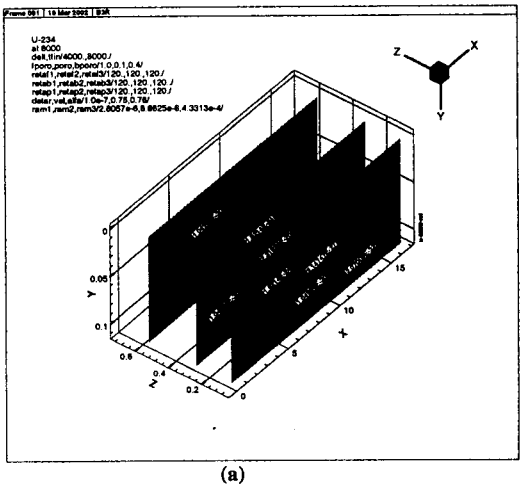

(a)

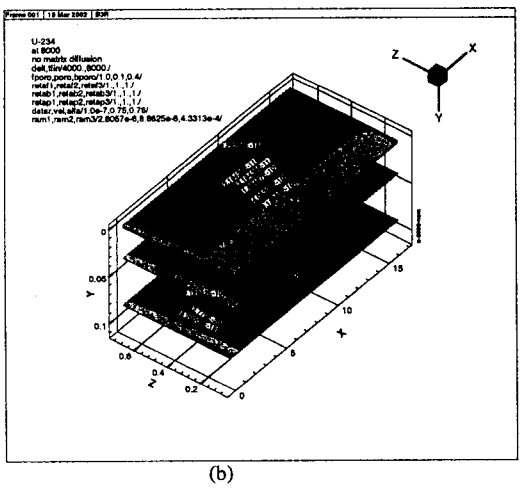

(b)

Fig. 12. Face Plots for ^{234}U at Time of 8×10^3 Years: (a) Retardation Considered; (b) No Matrix Diffusion Available

previous works associated with the control volume discretization, optimum temporal sizes as well as sufficient number of iterations for Gauss-Seidel Scheme have been obtained, even though the results are not shown again in this paper. Among these values some acceptable time steps are chosen.

To deal with interface diffusion coefficients, D_{f-p}, D_{b-p}, and D_{b-f} when the diffusion coefficients or dispersion coefficients are different in adjacent control volumes as in such cases as the fracture wall interfaced with the matrix and the buffer interfaced with rock, the analogy to a series of resistors can be utilized in the same way as discussed by Patankar (1980). Some more detailed discussions are to be found in Appendix II.

The same values of retardation factors for each medium of the buffer, the matrix and the fracture are used for simplicity, which does not seem to affect any illustrative purpose addressed by this study.

A three-dimensional model utilizing a control volume method and a computer code, B3R have been introduced for multi-member chain decay and transport through a fractured porous rock matrix.

For demonstration, transport behavior of nuclide having decay chains and its effect in the presence of buffer and rock matrix diffusion, considering in-growth due to daughter nucides' decay was investigated to show the importance of such barriers in view of HLW repository safety. Also to show three-dimensional visual transport behavior, some volume plots of parent nuclide, ^{234}U were introduced.

The model, which is an extension of previous work by Lee and Kang (1999a; 1999b) who developed the two-dimensional model for decay chain transport in a composite media of the buffer and the fractured porous medium is based on a physically exact formulation utilizing a control volume method and then the differential governing equation is directly integrated over each control volume. This kind of work believes to be very useful especially when a visualization is needed in order to represent the nuclide behavior around the canister and there needs a graphical representation of the nuclide behavior around the deep geological repository to investigate transport phenomena through the geologic media involved in the safety assessment of such repository and case studies to see what happens when varying properties of such barriers as the buffer and the rock matrix are applied to as well.

As noted before the main application of B3R is visualization of nuclide behavior in a fractured medium. Besides, as another important purpose of model development, currently KAERI (Korea Atomic Energy Research Institute) uses the MASCOT-K, developed in cooperation with AEA Technology, U.K. which is a one-dimensional PSA code to assess the overall safety of a potential repository in Korea. However, even though it is handy and versatile to accommodate many barriers into one overall model, it still has some restriction. One of the examples is simplification on the near field transport phenomena between buffer and a fracture surrounded by a porous medium. The current model in the MASCOT-K does not consider the following mechanisms:

(1) It does not estimate effects of any multi-dimensional transport inclusive of a finite volume of a fracture. In the MASCOT-K a fracture is infinitely wide.
(2) It does not consider any nuclide transfer from a buffer to an open fracture through surrounding host rock. If a fracture opening is very tight, then the transport from a buffer to a surrounding rock matrix cannot be underestimated any more, and
(3) It assumes parallel fractures only and cannot deal with any asymmetric fractures.

Probably, the current MASCOT-K approach might be conservative by simplifying these complicated issues. However, still, it may be worthwhile to understand detailed transport phenomena to support the validity of simplified MASCOT-K approaches. In addition, as currently planned, when KAERI actively develop the multi-dimensional PSA code to both calculate groundwater flow and nuclide transport, it need some comparable codes for code verification purpose and etc.

Using various computational results from B3R, real transport phenomena in a fracture are expected to be visualized not only for scientific communities but also for general public who still have negative feelings on the safety of a radioactive waste repository.

3. Appendix I

3.1. Three-Dimensional Discretization Equation

Designate the grid point in a control volume as P, with neighbors E and W in the x-direction, S and N in the y-direction, and B and F in the z-direction as shown in Fig. 4.

The control volume around P shown shaded in Figs. 4 and 5 has a volume of $\Delta x \times \Delta y \times \Delta z$ in a three-dimensional domain.

In order to avoid unrealistic results, it is convenient to consider the total flux due to advection plus dispersion in the fracture, utilizing an available analytical solution for the steady-state advection-dispersion equation, as introduced by Patankar (1980). This is called the "exponential scheme".

The governing equation for a steady state one-dimensional case in which the advection and dispersion terms are dealt with could be generally represented as

$$v\frac{dc}{dx}-\frac{d}{dy}\left(D_L\frac{dc}{dx}\right)=\frac{dJ}{dx}=0 \qquad \text{(A1)}$$

which has an exact solution for a domain $0 \le x \le (\delta x)_w$ (see Fig. 4(a)) subject to $c(0)=c_w$ and $c(x=(\delta x)_w)=c_p$ as

$$c(x)=c_w+(c_P-c_w)\times\left\{\frac{\exp(vx/D_L)-1}{\exp[v(\delta x)_w/D_L]-1}\right\} \qquad \text{(A2)}$$

which leads to the flux through the face e of the control volume having a grid point P

$$J_e=vc-D_L\frac{\partial c}{\partial x}=vc_E+\frac{v(c_E-c_P)}{\exp[v(\delta x)_e/(D_L)_e]-1}. \qquad \text{(A3)}$$

Similarly, for the flux through the face w,

$$J_w=vc-D_L\frac{\partial c}{\partial x}=vc_P+\frac{v(c_P-c_W)}{\exp[v(\delta x)_w/(D_L)_w]-1}. \qquad \text{(A4)}$$

Since the solution is obtained by marching forward in time, the discretization equations are derived by integrating Eqs. (1) and (2) over the control volume for node P and over the time interval Δt, which are represented as Eq. (A5) and (A6), respectively:

$$\int_t^{t+\Delta t}\int_f^b\int_s^n\int_w^e\left(R_l\frac{\partial c_l}{\partial t}+\lambda_l c_l R_l\right)dxdydzdt$$
$$=\int_t^{t+\Delta t}\int_f^b\int_s^n\int_w^e\left(\frac{\partial}{\partial y}\left\{D_{ly}\frac{\partial c_l}{\partial y}\right\}+\frac{\partial}{\partial z}\left\{D_{lz}\frac{\partial c_l}{\partial z}\right\}-\frac{dJ}{dx}+\lambda_{l-1}c_{l-1}R_{l-1}\right)dxdydzdt$$

$$\int_t^{t+\Delta t}\int_f^b\int_s^n\int_w^e\left(R_l^{b,p}\frac{\partial(\theta c_l)}{\partial t}+\lambda_l\theta c_l R_l^{b,p}\right)dxdydzdt$$
$$=\int_t^{t+\Delta t}\int_f^b\int_s^n\int_w^e\left(\frac{\partial}{\partial x}\left\{(\theta D_x^{b,p})\frac{\partial c_l}{\partial x}\right\}+\frac{\partial}{\partial y}\left\{(\theta D_y^{b,p})\frac{\partial c_l}{\partial y}\right\}\right.$$
$$\left.+\frac{\partial}{\partial z}\left\{(\theta D_y^{b,p})\frac{\partial c_l}{\partial z}\right\}+\lambda_{l-1}\theta c_{l-1}R_{l-1}^{b,p}\right)dxdydzdt$$

where J denotes the total flux, expressed as, $J = vc_l - D_L\frac{\partial c_l}{\partial x}$ which was discussed already.

By performing integration for a control volume, above Eq. (A5) can be evaluated as

$$\Delta x\Delta y\Delta z R_l\left\{{}_lc_P^{t+\Delta t}-{}_lc_P^{t}\right\}+\lambda_{l\,l}\,{}_lc_P^{t+\Delta t}\Delta t\Big\}=\Delta t\Delta z\Delta x D_{ly}\left[\frac{{}_lc_N^{t+\Delta t}-{}_lc_P^{t+\Delta t}}{(\delta y)_n}-\frac{{}_lc_P^{t+\Delta t}-{}_lc_S^{t+\Delta t}}{(\delta y)_s}\right]+$$
$$\Delta t\Delta x\Delta y D_{lz}\left[\frac{{}_lc_B^{t+\Delta t}-{}_lc_P^{t+\Delta t}}{(\delta z)_b}-\frac{{}_lc_P^{t+\Delta t}-{}_lc_F^{t+\Delta t}}{(\delta z)_f}\right]+\Delta t\Delta y\Delta z\left(J_e-J_w\right)-$$
$$-\lambda_{l-1}R_{l-1\,l}\,c_P^{t+\Delta t}\Delta x\Delta y\Delta z\Delta t.$$

Similarly, from Eq. (A6), difference equations can be obtained:

$$\Delta x\Delta y\Delta z\theta R_l^p\left\{{}_lc_P^{t+\Delta t}-{}_lc_P^{t}\right\}+\lambda_{l\,l}\,{}_lc_P^{t+\Delta t}\Delta t\Big\}=\Delta t\Delta y\Delta z R_l^p\left\{\theta D_x^p\right\}\left[\frac{{}_lc_E^{t+\Delta t}-{}_lc_P^{t+\Delta t}}{(\delta x)_e}-\frac{{}_lc_P^{t+\Delta t}-{}_lc_W^{t+\Delta t}}{(\delta x)_w}\right]$$
$$+\Delta t\Delta z\Delta x R_l^p\left\{\theta D_y^p\right\}\left[\frac{{}_lc_N^{t+\Delta t}-{}_lc_P^{t+\Delta t}}{(\delta y)_n}-\frac{{}_lc_P^{t+\Delta t}-{}_lc_S^{t+\Delta t}}{(\delta y)_s}\right]+\Delta t\Delta x\Delta y R_l^p\left\{\theta D_z^p\right\}\left[\frac{{}_lc_F^{t+\Delta t}-{}_lc_P^{t+\Delta t}}{(\delta z)_f}-\frac{{}_lc_P^{t+\Delta t}-{}_lc_B^{t+\Delta t}}{(\delta z)_b}\right]+$$
$$+\lambda_{l-1}\theta R_{l-1\,l-1}^p\,c_P^{t+\Delta t}\Delta x\Delta y\Delta z\Delta t.$$

Appendix II
Interface Diffusion Coefficients

As illustrated in Figs. 3 and 4, grid points are

always placed at the center of the control volumes. Therefore, when the control volume sizes are not uniform, their faces not lie midway between adjacent grid points. In these circumstances, Eq. (A9) can be used as the effective diffusion coefficient through the interface of the fracture and the matrix.

$$D_{f\to p}=\left(\frac{1-(\delta y)_{n+}/(\delta y)_n}{D_T}+\frac{(\delta y)_{n+}/(\delta y)_n}{(\theta_p D_y^p)}\right)^{-1} \qquad \text{(A9)}$$

where the distances are defined in Figs. 4 and 5(b).

In the same way, the effective diffusion coefficients through the interface of the buffer and the matrix ($D_{b\to p}$, $D_{p\to b}$) and the buffer and the fracture ($D_{b\to f}$, $D_{f\to b}$) can be obtained.

The interface diffusion coefficients, $D_{f\to p}$ and $D_{p\to f}$ should be the values replaced by (D_{ry}) in Eq. (1) and ($\theta_p D_y^p$) in Eq. (2), respectively. Similarly, $D_{b\to p}$ and $D_{p\to b}$ replaced by ($\theta_b D_x^b$) and ($\theta_p D_x^p$) in Eq. (2), and $D_{f\to b}$ and $D_{b\to f}$ replaced by (D_L) in Eq. (1) and ($\theta_b D_x^b$) in Eq. (2).

References

1. Final Storage of Spent Fuel:KBS-3, SKBF/KBS Report, Stockholm, Sweden, (1983).
2. Grisak, G.E. and J.F. Pickens, "Solute transport through fractured media: 1. The effect of matrix diffusion," *Water Resour. Res.*, 16(4), 719, (1980).
3. Gureghian, A.B., Analytical solutions for multidimensional transport of a four-member radionuclide decay chain in ground water, BMI/OCRD-25, (1987).
4. Harada *et al.*, Migration of radionuclides through sorbing media analytical solutions - I, ONWI-359, LBL-10500, UC-70, (1980).
5. Huyakorn, P.S. *et al.*, "An efficient finite element technique for modeling transport in fractured porous media, 1. Single species transport," *Water Resour. Res.*, 19(3) 841, (1983a).
6. Huyakorn, P.S. *et al.*, "An efficient finite element technique for modeling transport in fractured porous media, 2. Nuclide decay chain transport," *Water Resour. Res.*, 19(5) 1286, (1983b).
7. Kang, C.H., Mass transfer and transport of radionuclides through backfill in a geologic nuclear waste repository, Ph.D. Thesis, Chapter 2, University of California-Berkeley, (1989).
8. Kennedy C.A. and W.C. Lennox, "A control volume model of solute transport in a single fracture," *Water Resour. Res.*, 31(2) 313, (1995).
9. Lee Y.M. *et al.* "A Numerical Model for Nuclide Migration in the Far-field of the Repository," *J. Korean Nucl. Soc.*, 21(4), 267, (1989).
10. Lee, Y.M., *et al.*, "Continuous Time Markov Process Model for Nuclide Decay Chain Transport in the Fractured Rock Medium," *J. Korean Nucl. Soc.*, 25(4), 539, (1993).
11. Lee, Y.M. and K.J. Lee, "Nuclide Transport of Decay Chain in the Fractured Rock Medium: a Model Using Continuous Time Markov Process," *Ann. Nucl. Energy*, 22(2), 71, (1995).
12. Lee, Y.M., *et al.*, "A Stochastic Compartment Model for Nuclide Transport in the Fractured Porous Rock," Proc. of WM95, February 26 - March 2, 1995, Tucson, Arizona, U.S.A., (1995).
13. Lee, Y.M., *et al.*, "A nuclide Transfer Model for Barriers of the Seabed Repository Using Response Function," *J. Korean Nucl. Soc.*, 28(2), 539, (1996).
14. Lee, Y.M. and C.H. Kang, "A Method of Characteristics Solution of Nuclide Transport with Decay Chain," Proc. MRS'97:

International Symposium on the Scientific Basis for Nuclear Waste Management, Sept. 28-Oct. 3, 1997, Davos, Switzerland, (1997).

15. Lee, Y.M., *et al.*, "A Nuclide Decay Chain Transport Model by the Method of Characteristics," *J. Korean Nucl. Soc.*, 29(4), 539, (1997).
16. Lee, Y.M *et al.*, "Two-dimensional Nuclide Transport around a HLW Repository," *J. Korean Nucl. Soc*, 31(4), 432, (1999).
17. Lee, Youn-Myoung and Chul-Hyung Kang, "Two-dimensional Nuclide Decay Chain Transport in a Fractured Porous Medium by a Control Volume Approach," Annals of Nuclear Energy, 26, 1569, (1999a).
18. Lee, Youn-Myoung and Chul-Hyung Kang, "Two-dimensional Nuclide Decay Chain Transport around the Deep Geological Repository," Proc. Migration '99: Seventh International Conference in the Chemistry and Migration Behavior of Actinides and Fission Products in the Geosphere, Sept, 26-Oct. 1, 1999, Incline Village, Nevada/California, U.S.A., (1999b).
19. Lee, Youn-Myoung et al., "A Control-Volume Approach for Three-Dimensional Nuclide Transport around a Geological Repository," Proc. KNS Spring Meeting, 359, March 24-25, 2001, Cheju Univ. (2001).
20. Lung, H.-C., Migration of radionuclides through backfill in a nuclear waste repository, Ph.D. Thesis, Chapter 5, University of California-Berkeley, (1986).
21. Nerethieks, I., "Diffusion in the rock matrix: An important factor in radionuclide retardation?," *J. Geophys. Res.*, 85(B8) 4379-4397, (1980).
22. Patankar, S.V., Numerical Heat Transfer and Fluid Flow, Hemisphere, Washington, D.C., (1980).
23. Sudicky, E.A. and E.O. Frind, "Contaminant Transport in Fractured Porous Media: Analytical Solutions for a System of Parallel Fractures," *Water Resour. Res.*, 18(6), 1634, (1982).
24. Sudicky, E.A. and E.O. Frind, "Contaminant Transport in Fractured Porous Media: Analytical Solution for a Two-Member Decay Chain in a Single Fracture," *Water Resour. Res.*, 20(7), 1021, (1984).
25. Yamashita R. and H. Kimura, "Particle-tracking technique for nuclide decay chain transport in fractured porous media," *J. Nucl. Sci. Tech.*, 27(11), 1041, (1990).